Journal of
Scientific Conference Proceedings
Vol. 1, 7–14, 2008

RESEARCH ARTICLE

Preparation, Characterization and Catalytic Activity of Transition Metal Oxide Nanocrystals

Gurdip Singh*,[1], I. P. S. Kapoor[1], Shalini Dubey[1], and Prem Felix Siril[2]

[1]Chemistry Department, D. D. U. Gorakhpur University, Gorakhpur– 273009, India
[2]University of Hudderfield, Hudderfield, HD1 3DH, UK

Nanocrystals of four transition metal oxides (TMOs) were prepared by a novel quick precipitation method and characterized by X-ray diffraction (XRD) and transmission electron microscopy (TEM). From the XRD patterns, average particle sizes for CuO, NiO, Co_2O_3, MnO_2 are calculated to be 15 nm, 4 nm, 13 nm, 40 nm, respectively. The TEM study revealed that the majority of CuO particles are of 6–8 nm in size. Catalytic activities of the TMO nanocrystals for thermal decomposition of ammonium perchlorate (AP) were investigated using differential thermal analysis (DTA), thermogravimetric analysis (TGA) and ignition delay measurements. The order of catalytic activity of these oxide nanocrystals on thermal decomposition of AP was found to be: $Co_2O_3 > CuO > NiO > MnO_2$.

Keywords: Transition Metal Oxide Nano Crystal (TMONC), Ammonium Perchlorate, Catalytic Activity, Thermal Decomposition.

1. INTRODUCTION

Metal oxides are an important class of chemicals having wide-ranging applications in many areas of chemistry, physics and material science.[1–5] In technological applications, metal oxides are used in the fabrication of micro-electronic circuits, sensors, fuel cells, and as catalysts.[6] In the emerging field of nanotechnology, one goal is to make nanostructures with special properties with respect to those of bulk species.[7–11] Metal oxide nanocrystals can exhibit unique physico-chemical properties due to their nano size and high density of cover or edge surface sites.

Transition metal oxides (TMOs) have received considerable attention in recent years for their catalytic, electronic and magnetic properties.[12–14] Nano meter-sized metal oxides are expected to possess better properties than those of bulk metal oxides.[15–17] There are many routes for the preparation of transition metal oxide nanocrystals (TMONC). Generally, an appropriate salt of the transition metal is oxidized by chemical or thermal treatments to yield the corresponding metal oxide, and the size of the resultant TMO can be controlled kinetically or thermodynamically (by using templates). In recent years, methods have been developed for the preparation of novel nano structure of metal oxides. They can be generated by a number of preparative methods that typically are described as physical and chemical methods.[18, 19] Conventional methods for the preparation of metal oxide powder include one-step solid state reaction at room temperature, thermal decomposition of metal salts, mechanical milling of commercial powders, and so on.[20–22] However, none of these methods seems to be suitable for the preparation of highly dispersed oxide nanocrystals, which has been found to be an obstacle to many applications, especially in catalysts and electrode.[23, 24] Recently several new approaches have been developed with the aim of obtaining well-dispersed oxide nanocrystals. Nevertheless, few methods reported for preparation of TMONC required large amounts of organic solvents and expensive ultrasonic equipment.[25, 26] Now it becomes necessary to adopt a very easy and low cast preparation method of TMONC. Therefore, in the present communication, preparation of metal oxide nanocrystals (CuO, NiO, Co_2O_3 and MnO_2) has been carried out via a novel quick precipitation method.[27] The size of the nanocrystals is controlled in this route by kinetic control, as the name suggests. We have characterized the four TMO using powder XRD, TEM and surface area measurements, and the results suggest that TMOs produced are having sizes in the nanometer range.

Ammonium perchlorate is the most common oxidizer in composite solid propellants (CSPs). Thermal decomposition characteristics of AP influence the combustion behavior of the propellants.[28] AP based composite solid propellants require combustion modifiers to achieve higher burning rates,

*Author to whom correspondence should be addressed.

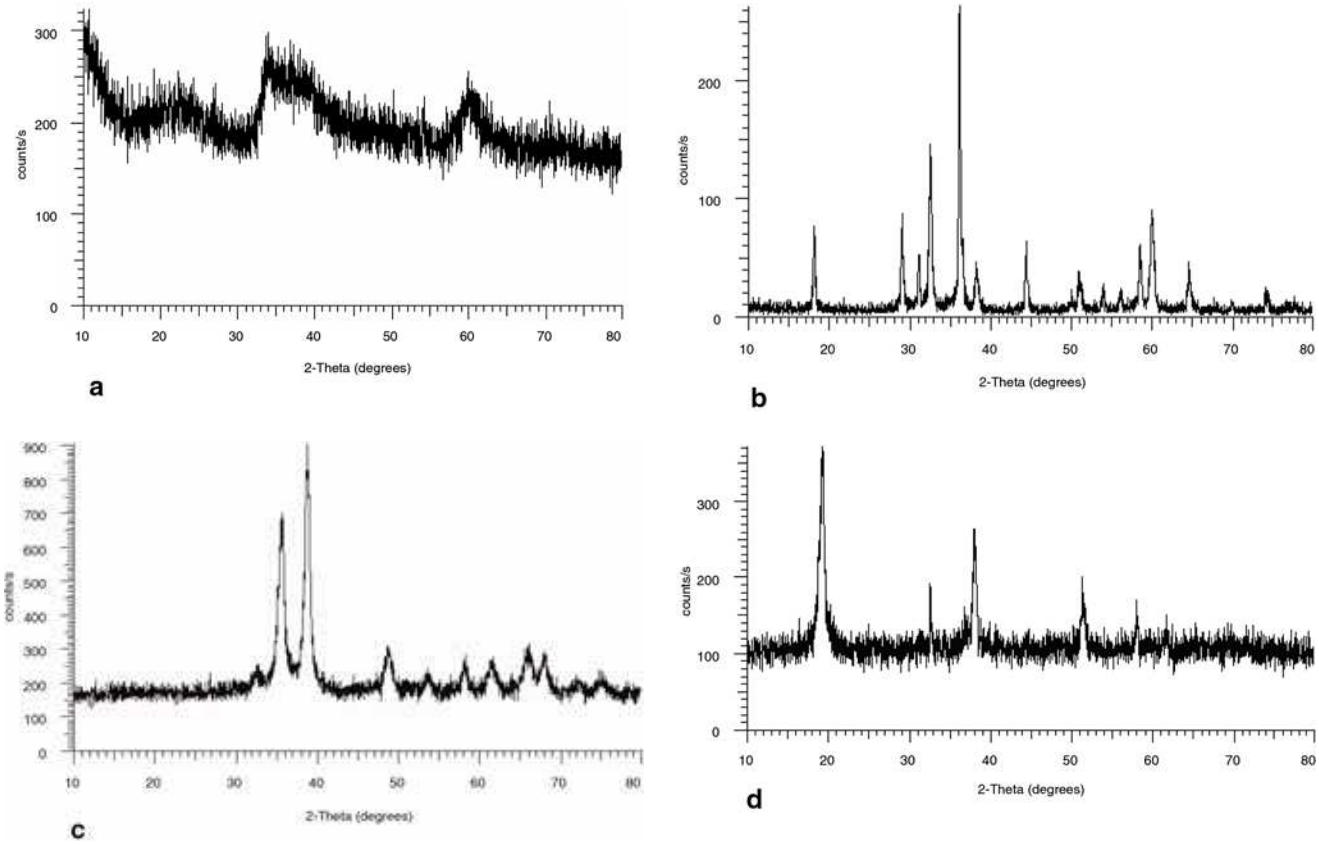

Fig. 1. XRD pattern for TMONC (a) NiO (b) MnO_2 (c) CuO (d) Co_2O_3.

and conventional TMOs are used as the burning rate modifiers.[12] Our group is involved in the development of burning rate modifiers for AP based composite solid propellants.[28–30] Our previous studies suggested that the burning rate modifiers are active mainly in the condensed phase, and hence, activity of the catalysts during condensed phase thermolysis of AP can be a good indicator to the catalytic activity of the additive during combustion of CSPs.[28] The catalytic activity of transition metal oxide in the thermal decomposition of AP has been reported.[28–32] It is generally observed that since catalytic activity is primarily a surface phenomenon, size reduction of the catalyst increases the surface area and hence the catalytic activity is also increased. Activities of the solid catalysts increase manifold by size reduction into the nanometer scale.[33–35]

2. EXPERIMENTAL

2.1. Materials

Ammonium perchlorate obtained from CECRI, Karaikudi was used as such without further purification. Crystals of AP were ground into fine powder using a pestle and mortar and sieved to 100–200 mesh. Acetates of Cu, Ni, Co, Mn and acetic acid were from sd-fine chemicals Ltd. and NaOH was from Merck. All these chemicals were used as received.

2.2. Preparation of Metal Oxide Nanocrystals

All of the metal nanocrystals were prepared by a novel quick precipitation method, as reported earlier,[27] which involves mixing a corresponding metal acetate aqueous solution to glacial acetic acid under reflux condition, followed by addition of NaOH at 100 °C until the pH was 6–7. After being cooled to room temperature, the precipitate was centrifuged, washed once with distilled water and three times with absolute ethanol, respectively, and dried in air at room temperature.

2.3. Characterization

XRD measurements were performed on the TMO nanocrystals by an advanced X-ray diffractometer using CuKα radiation (λ =1.5418). The diffraction patterns are shown in Figure 1. Particle size of the crystals was calculated by applying Scherrer's formula[36, 37] to the powder XRD data, and the values are reported in Table I. TEM images on CuO were obtained by using instrument, Tecnai GZ 20(FEI make),

Table I. Crystal size, surface area, pore volume and pore size of TMONC by nitrogen porosimetry.

Sample	Crystal size[a]/nm	Surface area[b]/m^2 g^{-1}	Pore volume[c]/cm^3 g^{-1}	Pore size[d]/nm
CuO	15	57.47	0.328	19.426
NiO	4	163.74	0.061	3.218
MnO_2	40	28.55	0.146	19.163
Co_2O_3	13	212	0.012	4.000

[a] Calculated using the Scherrer's formula on the diffraction peak of maximum intensity.
[b] From BET equation.
[c] Total volume of pores using BJH equation during adsorption.
[d] From BJH equation during adsorption.

at operating voltage 200 KV. A representative micrograph and the corresponding electron diffraction pattern are shown in Figures 2a and 2b, respectively. Surface area, pore volume, and pore size were measured by N_2 porosimetry using a Micrometrics ASAP 2020 instrument. All of the catalysts were degassed at 250 °C, and then N_2 adsorption and desorption were performed and isotherms were recorded at 77K. Surface area was calculated using the BET equation. Both adsorption and desorption data were used to calculate the pore volume using the BJH equation, and good agreements were obtained. Pore diameter was also calculated

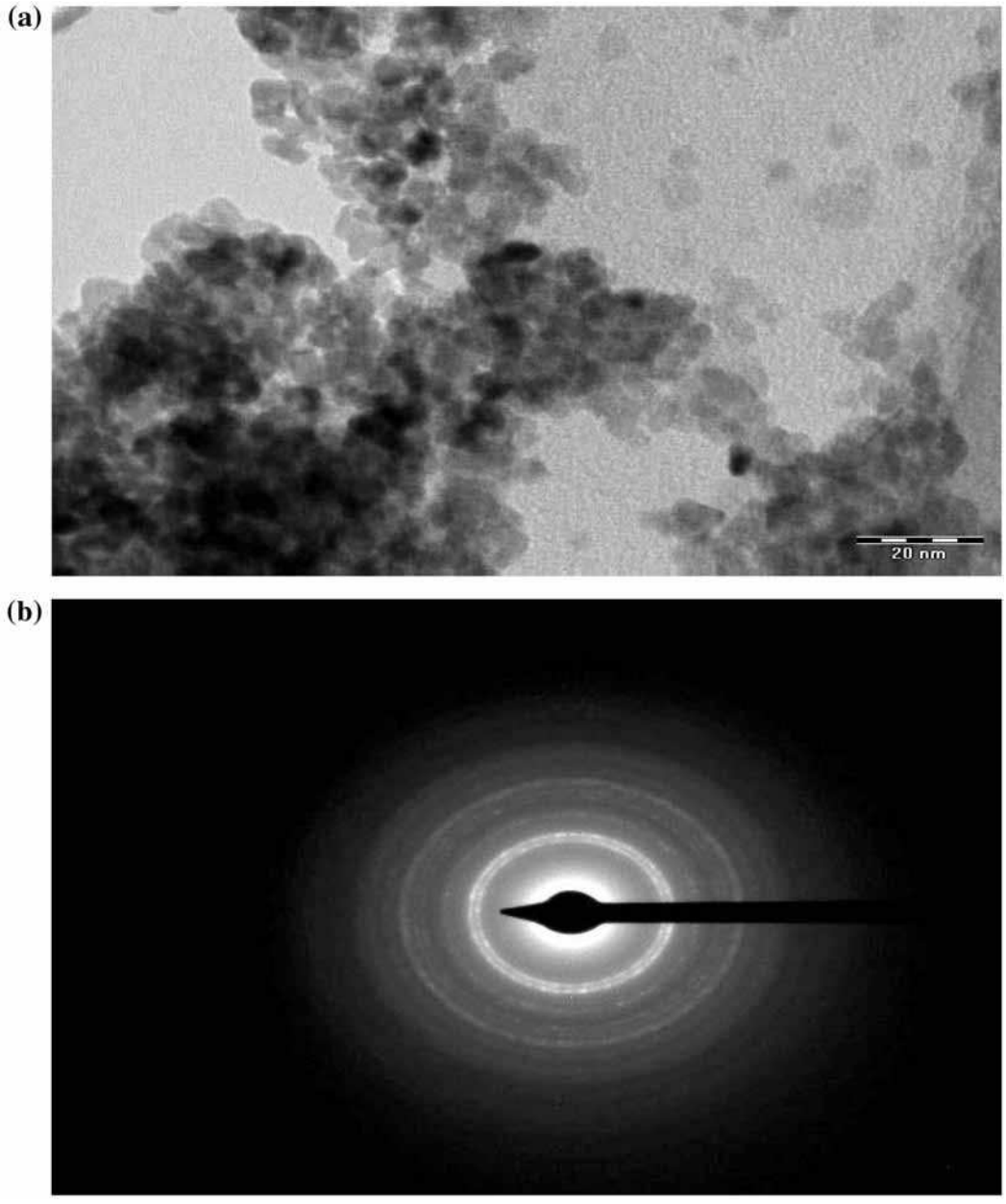

Fig. 2. (a) TEM image of CuO. (b) ED pattern of CuO.

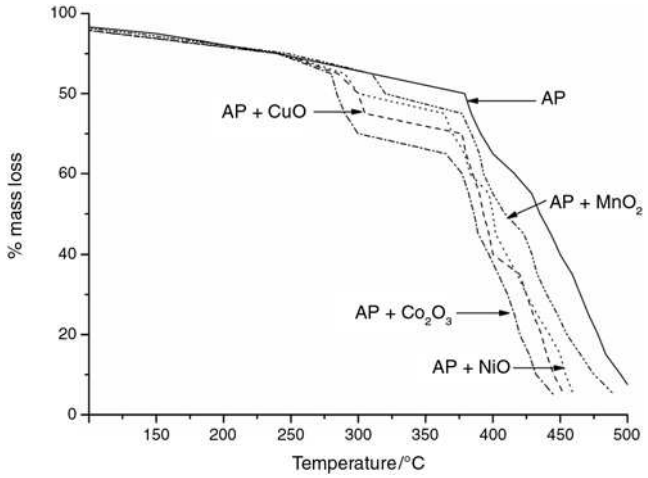

Fig. 3. Non-isothermal TG thermal curves of AP and its mixtures with TMONC (1% by mass) at 10 °C min^{-1} under air atmosphere. Name of each TMO is clearly marked on the curves.

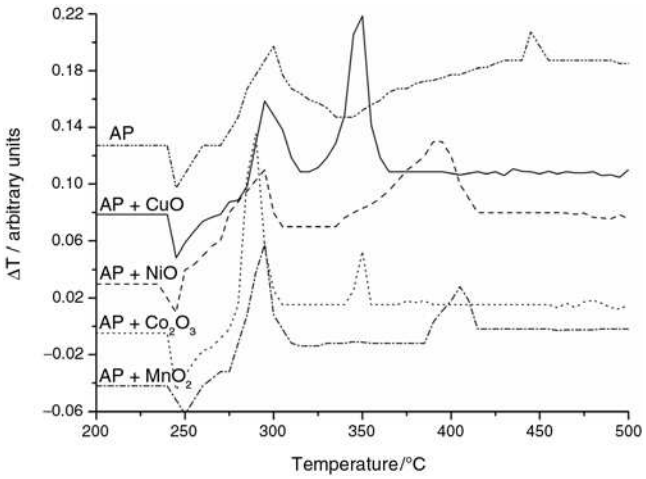

Fig. 4. DTA thermal curves of AP and its mixtures with TMONC (1% by mass) at 10 °C min^{-1} under air atmosphere. Name of each TMO is clearly marked on the curves.

using BJH method. The results of nitrogen porosimetry are reported in Table I.

2.4. Catalytic Activity Measurements During Thermal Decomposition of AP

Catalytic activities of the prepared TMO nanocrystals for thermolysis of AP were studied using a number of thermoanalytical techniques, such as non-isothermal and isothermal TG, DTA and by measuring the ignition delay (D_i) after mixing 1% by mass of TMOs with AP. Non-isothermal TG thermal curves were recorded on the samples (~ 20 mg) using an indigenously fabricated apparatus[38] at a heating rate of 10 °C min^{-1} under static air atmosphere. The non-isothermal TG thermal curves are shown in Figure 3. DTA thermal curves were recorded on Universal Thermal Analysis Instrument, Mumbai, under static air atmosphere at a heating rate of 10 °C min^{-1} and the thermal curves are shown in Figure 4. Isothermal TG thermal curves were recorded at 260 °C under static air atmosphere and the corresponding thermal curves are shown in Figure 5. Rate of decomposition of pure and catalysed AP at 25% mass loss were calculated and the values are reported in Table II.

Ignition delays of AP with and without TMO nanocrystals were measured by using the tube furnace technique (TF).[39] A small sample (~ 20 mg) was taken in an ignition tube (length 5 cm and diameter 0.4 cm), clamped with bent wire and inserted manually into the tube furnace. The time interval between the insertion of the ignition tube into the TF and the moment of visible ignition, noted with the help of a stop watch, gave the value of ignition delay in seconds. The accuracy of the temperature of TF was ± 1 °C. Each run was reported four times, and mean D_i values are reported in Table III. The D_i data were found fit in following equation[40, 41]

$$D_i = A\, e^{E^*/RT}$$

where E* is the activation energy for ignition and T, the absolute temperature. The plots of ln D_i versus 1/T are presented in Figure 6.

The effect of the amount of catalyst on the catalytic activities was further analyzed using isothermal TG of samples with varying composition. Isothermal TG thermal curves were recorded on samples of AP containing 2, 1, 0.5 and 0.25% by mass of TMO nanocrystals at 260 °C under static air atmosphere, and thermal curves are also shown in Figure 5.

3. RESULTS AND DISCUSSION

Powder XRD patterns reported in Figure 1 match well with the reported XRD patterns in the literature for these four TMOs. The XRD patterns for all TMOs except that for NiO show considerable broadening of the peaks, and such broadening is known as due to the presence of very small crystallites. Particle size of these very small crystallites, reported in Table I, shows that the prepared TMOs are in the nanometer range. NiO shows relatively sharp peaks in comparison to the other three TMOs as it has slightly larger particle size. We have further substantiated this claim by transmission electron microscopy of CuO. Particle size of CuO nanocrystals, as observed in TEM image (Fig. 2), is slightly lower than the size calculated from XRD. Such difference is agreeable as we can only calculate an average value only from XRD even if there is some distribution in particle size; moreover, it is inferred that TMONC prepared, although under identical conditions with the same method but in different batches, may lead to different nanorange particle

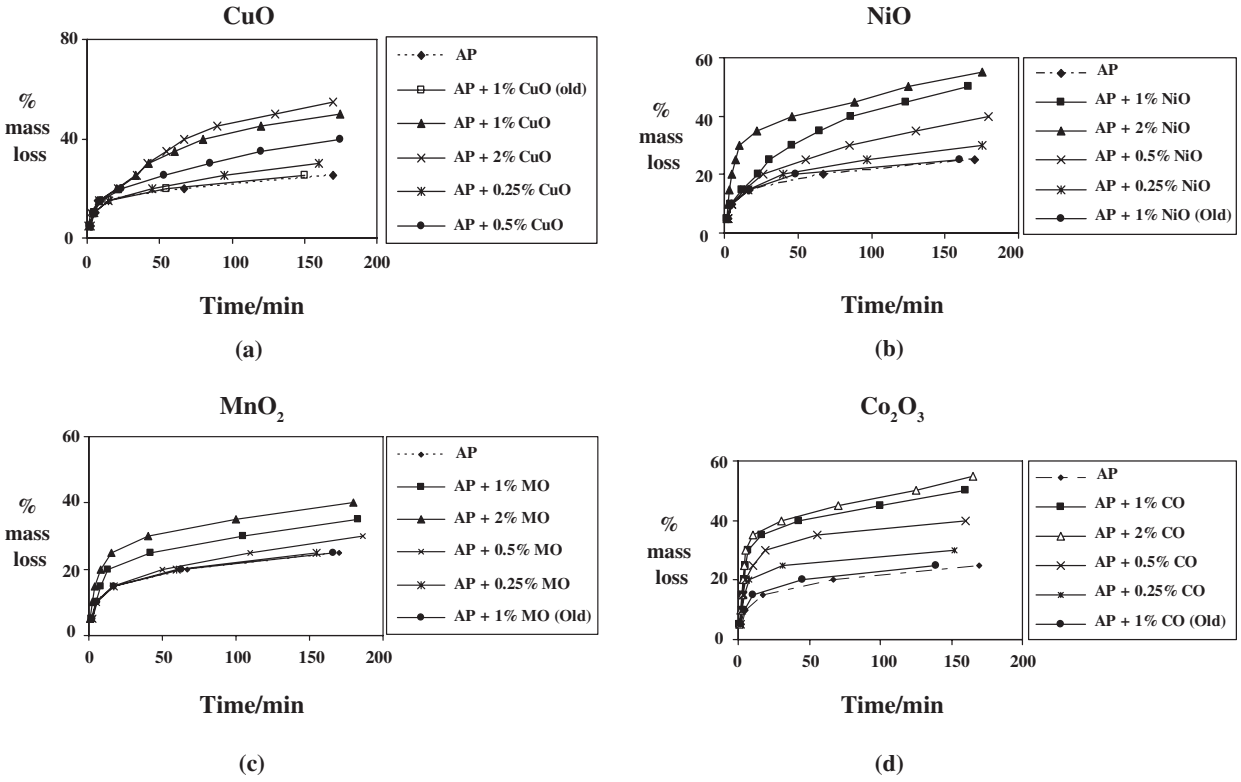

Fig. 5. Isothermal TG of various % of TMONC in AP at 260 °C where MO for MnO_2, CO for Co_2O_3.

Table II. Decomposition rate and catalytic activity of AP, AP + TMONC and AP + TMO (old).

Sample	Temperature (°C)	Decomposition Rate (for 25% decomposition min^{-1}) of TMONC	Decomposition Rate (for 25% decomposition min^{-1}) of TMO (old)	C_A (Catalytic activity) of TMONC	C_A (Catalytic activity) of TMO (old)
AP	260	0.142	0.142	—	—
AP + CuO (1% wt)	260	0.819	0.167	5.77	1.174
AP + NiO (1% wt)	260	0.745	0.156	5.25	1.100
AP + Co_2O_3 (1% wt)	260	1.600	0.180	11.27	1.268
AP + MnO_2 (1% wt)	260	0.595	0.151	4.19	1.062

Table III. Ignition delay (D_i), Activation energy for ignition (E*) and correlation coefficient of AP and AP + TMONC.

	D_i (Sec.)							
Sample	300 ±1 °C	310 ±1 °C	320 ±1 °C	330 ±1 °C	340 ±1 °C	E (KJ/mol)	r (Correlation coefficient)	In A
AP	150	137	119	101	85	42.01	0.9913	0.000762
AP + CuO (1% wt)	88	76	64	61	54	35.05	0.9980	0.000710
AP + NiO (1% wt)	92	85	70	64	58	35.29	0.9904	0.000696
AP + Co_2O_3 (1% wt)	85	71	62	58	53	33.60	0.9847	0.000686
AP + MnO_2 (1% wt)	96	88	74	67	60	35.45	0.9952	0.000681

size. This fact has also been reported by some workers.[27] TEM imaging was not possible on the other three TMOs, due to their high magnetic property.

Non-isothermal TG thermal curve and characteristic temperatures for thermolysis of pure AP, as shown in Figure 3, are comparable to the well-established thermal decomposi-

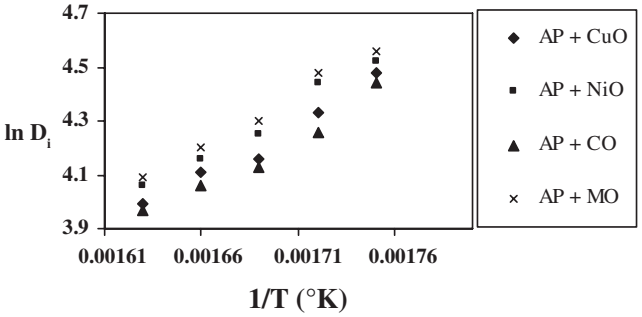

Fig. 6. Plots of ln D_i vs 1/T for 1% TMONC in AP where CO for Co_2O_3, MO for MnO_2.

tion pattern for this compound. It is well-known that mass loss for AP takes place in two steps.[42, 43] AP on heating first loses ~ 25% of its mass at around 250 °C, and this is usually called low temperature decomposition (LTD). A plateau is observed in the TG thermal curve beyond this temperature, and AP loses almost all its mass at around 450°C. This process is called high temperature decomposition (HTD). It can be seen from Figure 3 that the catalysts affect both LTD and HTD of AP. Higher percentage mass loss is observed in the thermal curves for AP+TMO mixtures than that for pure AP. Onset temperatures for HTD for the mixtures are considerably lower than that for pure AP. Gasification of AP in the presence of catalysts during HTD not only begins early, but also completes at lower temperatures. Thus, endset temperatures of about 505 °C, 490 °C, 460 °C, 453 °C, 445 °C were observed for AP, AP+MnO_2, AP+NiO, AP+CuO and AP+Co_2O_3, respectively.

The first feature in the DTA thermal curve for pure AP is an endothermic peak at 245 °C, and this represents the polymorphic transition from orthorhombic to cubic.[44] This endothermic process is followed by an exothermic peak at ~ 300 °C, and this corresponds to LTD. A second exothermic peak was found at ~ 445 °C associated with HTD.[42–44]

As shown in Figure 4 (ΔT, the difference between temperature of reference and sample vs temperature), DTA thermal curves for decomposition of AP in the presence of metal oxide nanocrystals show noticeable changes in the decomposition pattern. The three characteristic peaks are visible in the DTA thermal curves for the mixtures of AP with the TMOs. The endothermic peak corresponding to the polymorphic transition is observed at 245 °C for AP and its mixtures with TMOs. The peak temperature corresponding to the LTD process also is not altered considerably for the mixtures. However, the peak temperatures corresponding to the HTD process for the mixtures were observed at considerably lower temperatures, indicating the effect of the catalysts.

Thus, the non-isothermal TG and DTA results clearly show that all four TMO nanocrystals do catalyze the thermolysis of AP in their mixtures. In order to quantify the catalytic activities of these TMOs (for both TMONC & TMOC), we have further recorded isothermal TG thermal curves of AP and its mixtures with the TMOs (1% by mass). The rates of decomposition at 25% mass loss of AP and its mixtures with the catalysts have been calculated from the isothermal TG curve shown in Figure 5, and the values are given in Table I. The catalytic activity (C_A) of these catalysts has been estimated by using the following equation:

$$\text{Catalytic activity } (C_A) = C_0/C$$

where C_0 is rate of decomposition of catalyzed AP and C is rate of decomposition of uncatalyzed AP.

Although bulk size (old) TMO also catalyzes the thermal decomposition of AP, it has been observed (Fig. 5, Table I) that TMONC were found to enhance the thermal decomposition of AP comparatively to greater extent. It is inferred that this fact could be due to the nanosize of the oxides. The order of catalytic activity for AP thermal decomposition was found to be:

$$Co_2O_3 > CuO > NiO > MnO_2$$

The isothermal TG curve presented in Figure 4 for various compositions of metal oxide in AP clearly shows that increase of metal oxide nanocrystal content may increase the thermal decomposition of AP. Thus, the order of catalytic effect with increase of metal oxide nano crystal content in AP was found to be:

$$2\% > 1\% > 0.5\% > 0.25\% \text{ (\% by wt in AP).}$$

We have further substantiated the catalytic activities of the TMO nanocrystals for thermolysis of AP by measuring the ignition delay of AP in the presence of these catalysts. AP in the presence of TMO nanocrystal (1% by mass) as catalyst ignites with noise and fumes under rapid heating. Ignition delay data (300 °C–340 °C) in Table III show that the time required for ignition at fixed temperature increases in order: AP < AP + Co_2O_3 < AP + CuO < AP + NiO < AP + MnO_2. It can also be seen from Table III that the activation energy for thermal ignition for pure AP is lowered by the catalysts in their mixtures with AP. The kinetic parameters and correlation coefficient are presented in Table III. This result clearly indicates that these metal oxide nanocrystals act as a good catalyst during deflagration of AP with decreasing activation energy for ignition. The order of catalytic activity observed during thermal ignition was as follows:

$$Co_2O_3 > CuO > NiO > MnO_2.$$

The mechanism of catalyzed AP thermal decomposition can be understood by the electron-transfer process. The present TG data are recorded below 300 °C, and it is known that AP thermal decomposition takes place by the electron transfer process in this temperature range. It is possible that metal oxide enhances the decomposition of AP, on account of their increased electron hole density as has been suggested by Solymosi et al.[45, 46] The presence of a partially filled 3d-

orbital may provide help in the electron-transfer process. A positive hole in oxide can accept an electron from perchlorate.

Although the present study involves only one nanorange of a particular TMO, it is a well-known fact that the smaller the size of a crystal, the more enhanced its catalytic effect would be.

4. CONCLUSIONS

TMONC were prepared by a novel quick precipitation method (kinetic method) and characterized by XRD and TEM techniques. Their catalytic activity on thermal decomposition of AP was studied, and they have been found to be good catalysts, as compared to their corresponding normal oxides. The order of the catalytic effect of TMONC in the thermal decomposition of AP is:

$$Co_2O_3 > CuO > NiO > MnO_2.$$

With the increase in content of nanosized metal oxide in AP, enhancement in catalytic activity occurs.

Acknowledgments: The authors are grateful to the head of the Chemistry Department of D. D. U. Gorakhpur University for its laboratory facility. The authors are highly thankful to Dr. Ajay Gupta (Director) and Dr. N. P. Lalla of CSR, Indore, for the TEM images.

References

1. C. Nogeura, Physics and Chemistry at Oxide Surface, Cambridge University Press, Cambridge, UK (**1996**).
2. H. H. Kung, Transition Metal Oxides: Surface Chemistry and Catalysis, Elsevier, Amsterdam (**1999**).
3. V. E. Henrich and P. A. Cox, The Surface Chemistry of Metal Oxides, Cambridge University Press, Cambridge, UK (**1994**).
4. A. F. Wells, Structural Inorganic Chemistry, 6th ed., Oxford University Press, New York (**1987**).
5. W. A. Harrison, Electronic Structure and the Properties of Solids, Dover, New York (**1989**).
6. Handbook of Heterogenous Catalysis (G. Eetl, H. Knozinger; and J. Weitkamp, Eds.). Wiley-VHC, Weinheim (**1997**).
7. H. Gleiter, *Nanostructured Mater.* 6, 3 (**1995**).
8. J. A. Rodriguez, G. Liu, T. Jirsak, et al. *J. Am. Chem. Soc*. 124, 5247 (**2002**).
9. M. Baumer and H. J. Freund, *Prog, Surf. Sci*. 61, 127 (**1999**).
10. M. L. Trudeau and J. Y. Ying, *Nanostrutured Mater.* 7, 245 (**1996**).
11. M. Valden, X. Lai, and D. W. Goodman, *Science* 281, 1647 (**1998**).
12. C. L. Carnes and K. J. Klabunde, *J. Mol, A Catal, Chem*. 194, 227 (**2003**).
13. V. Biju and M. Abdul Khader, *Mater. Sci. Eng*., A 304–306, 814 (**2001**).
14. Y. Ichiyanagi, N. Wakabayashi, J. Yamazaki, et al. *Physica B* 329–333, 862 (**2003**).
15. L. Lw, Y. Wu, Y. Shi, and C. Hu, *Mater. Lett*. 58, 2700 (**2004**).
16. D. L. Tao and F. Wei, *Mater. Lett*. 58, 3226 (**2004**).
17. V. Biju and M. Abdul Khader, *Spectrochim. Actaa Part A* 59, 121 (**2003**).
18. Nanomaterials; Synthesis, Properties and Application (A. S. Edelstein and R. C. Cammarata, Eds.). In statute of physics Publishing, London (**1998**).
19. A. Khaleel and R. M. Richards, in: Nanoscale Materials in Chemistry (K. J. Kladunde, Ed.). Wiley, New York (**2001**), Chapter 4.
20. J. F. Xu, W. Ji, Z. X. Shen, et al. *J. Solid state Chem*. 147, 516 (**1999**).
21. C. Carel, M. M. Bahout, and J. C. Gaude, *Solid State Ionics* 117, 47 (**1999**).
22. R. A. Borzi, S. J. Stewart, R. C. Mercader, G. Punte, and F. Garcia, *J. Magn. Mater.* 226–230, 1513 (**2001**).
23. S. Bennici, A. Gervasini, and V. Ragaini, *Ultrason. Sonochem*. 10, 61 (**2003**).
24. T. Y. You, O. Niwa, M. Tomita, H. Andoo, M. Suzuki, and S. Hirono, *Electorchem. Commun*. 4, 468 (**2002**).
25. Z. S. Hong, Y. Cao, and J. F. Deng, *Mater. Lett*. 52, 34 (**2002**).
26. R. V. Kumar, Y. Diamant, and A. Grdanken, *Chem. Mater* 12, 34 (**2000**).
27. J. Zhu, D. Li, H. Chen, X. Yang, L. Lu, and X. Wang, *Mater. Lett*. 58, 3324, (**2004**).
28. G. Singh and S. P. Felix, *Combust. Flame* 132, 422 (**2003**).
29. K. Kishore and M. R. Sunitha, *AIAA J.* 17, 1118 (**1979**).
30. G. Singh and D. K. Pandey, *J. Energ. Mater.* 20, 223 (**2002**).
31. N. B. Singh and A. K. Ojha, *Thermochim. Acta*.390, 67 (**2002**).
32. A. A. Said and R. Al-Qusami, *Thermochim. Acta*. 275, 83 (**1996**).
33. J. Zhu, H. Chen, B. Xie, X. Yang, L. Lu, and X. Wang, Chin, *J. Catal* 25, 637 (**2004**).
34. J. Zhu, W. Zhang, H. Wang, et al. *J. Inorg. Chem*. 20, 863 (**2004**).
35. Z. Ma, F. Li, A. Chen and H. Bai, *Acta Chim, Sin*.13, 1252 (**2004**).
36. L. S. Birks and H. Fridman, *J. Appl, Phys*.17, 687 (**1946**).
37. W. A. Rosser and S. H. Inami, *Combust. Flame* 12, 427 (**1968**).
38. G. Singh and I. P. S. Kapoor, *J. Energ.; Mate*. 11, 293 (**1993**).
39. G. Singh, R. R. Singh, A. P. Rai, and I. P. S. Kapoor, *J. Therm. Anal*. 36, 2539 (**1990**).
40. N. Semenov, Chemical Reactions, Clarendon Press, Oxford (**1935**), Chapter 18.
41. E. S. Feeam and S. Gorden, *J. Phys. Chem*. 60, 867 (**1956**).
42. P. W. M. Jacobsete, *Combust., Flame* 13, 419 (**1969**).
43. F. Solymosi, *Acta. Phys. Chem*. 20, 1 (**1974**).
44. K. Kishore and K. Sridhara, Solid propellant chemistry: condensed phase behavior of ammonium perchlorate based solid propellants, DESIDOC, New Delhi (**1999**), p.10.
45. F. Solymosi, *Acta. Phys, Chem*. 20, 1 (**1974**).
46. F. Solymosi and K. Fanagy, Eleventh International Symposium on Combustion, The Combustion Institute, Pittsburgh (**1967**), 425.

Received: 29 January 2007. Accepted: 18 December 2007.